Journal of Computational Neuroscience (2019) 46:77–90
https://doi.org/10.1007/s10827-018-0686-8

Linear feature projection-based real-time decoding of limb state from dorsal root ganglion recordings

Sungmin Han[1] · **Jun-Uk Chu**[2] · **Jong Woong Park**[3] · **Inchan Youn**[1,4]

Received: 25 October 2017 / Revised: 26 April 2018 / Accepted: 30 April 2018 / Published online: 15 May 2018

Abstract

Proprioceptive afferent activities recorded by a multichannel microelectrode have been used to decode limb movements to provide sensory feedback signals for closed-loop control in a functional electrical stimulation (FES) system. However, analyzing the high dimensionality of neural activity is one of the major challenges in real-time applications. This paper proposes a linear feature projection method for the real-time decoding of ankle and knee joint angles. Single-unit activity was extracted as a feature vector from proprioceptive afferent signals that were recorded from the L7 dorsal root ganglion during passive movements of ankle and knee joints. The dimensionality of this feature vector was then reduced using a linear feature projection composed of projection pursuit and negentropy maximization (PP/NEM). Finally, a time-delayed Kalman filter was used to estimate the ankle and knee joint angles. The PP/NEM approach had a better decoding performance than did other feature projection methods, and all processes were completed within the real-time constraints. These results suggested that the proposed method could be a useful decoding method to provide real-time feedback signals in closed-loop FES systems.

Keywords Linear feature projection · Projection pursuit · Negentropy maximization · Proprioceptive afferent · Kalman filter

1 Introduction

Proprioception is the sense of position and movement of the body, which plays an important role in the planning and execution of motor control, in which natural motor functions are controlled based on the sensory-to-motor transformation (Prochazka 2015; Wolpert and Ghahramani 2000). Many studies have been performed to discover how to generate a motor command based on sensory information to achieve complex and natural control in functional electrical stimulation (FES) systems. For example, proprioceptive afferent activities have been recorded from dorsal root ganglia and used to decode limb positions induced by passive movements (Rigosa et al. 2011; Stein et al. 2004; Wagenaar et al. 2011; Weber et al. 2007) and active movements (Rigosa et al. 2011; Weber et al. 2006;

Action Editor: Byron Yu

Sungmin Han and Jun-Uk Chu contributed equally to this work.

✉ Jong Woong Park
ospark@korea.ac.kr

✉ Inchan Youn
iyoun@kist.re.kr

Sungmin Han
han0318@kist.re.kr

Jun-Uk Chu
juchu@kimm.re.kr

[1] Biomedical Research Institute, Korea Institute of Science and Technology, 5, Hwarang-ro 14-gil, Seongbuk-gu, Seoul, 02791, Republic of Korea

[2] Daegu Research Center for Medical Devices and Rehabilitation Engineering, Korea Institute of Machinery and Materials, 330, Techno Sunhwan-ro, Yuga-myeon, Dalseong-gun, Daegu, 42994, Republic of Korea

[3] Department of Orthopedic Surgery, Korea University College of Medicine, 73, Inchan-ro, Seongbuk-gu, Seoul, 02841, Republic of Korea

[4] Division of Bio-Medical Science and Technology, KIST School, Korea University of Science and Technology, 5, Hwarang-ro 14-gil, Seongbuk-gu, Seoul, 02791, Republic of Korea

2007). Dorsal root ganglion recordings were also used to provide closed-loop control limb positions in FES systems (Bruns et al. 2013; Holinski et al. 2013). Sensory information derived from proprioceptors can be obtained using microelectrodes placed at the dorsal root ganglion, in which the cell bodies of sensory neurons are located. This approach, which can provide an abundance of sensory information at a single location, has an advantage compared with other central or peripheral recording locations.

Neural activities of multiple neurons in the peripheral or central nervous systems recorded by microelectrodes are classified into single-neuron spikes for further analysis, in which the spikes are characterized by statistical measures of interest, such as temporal code (i.e., the precise timing of spikes provides the temporal structure of a spike train) and rate code (i.e., the number of spikes provides the spike frequency) (Cunningham et al. 2009; Pregowska et al. 2016). The recent development of high-density microelectrodes has enabled simultaneous extracellular recordings from up to 100 electrodes, which could represent hundreds of active neurons. As the number of simultaneously recorded neurons increases, the computational complexity increases, and advanced algorithms are required. Consequently, it is important to produce low-dimensional representations that preserve the feature of interest from the large scale of neural data to reduce computational effort and processing time (Cunningham and Byron 2014). In previous studies, feature projection has been applied to reduce the dimensionality of the feature vectors. For example, the response of a neural population in the motor cortex of monkeys was projected using a principal component analysis (PCA) to determine the relevant dynamical structure of reaching movements, wherein the dimensions of the neural response were reduced to the six response patterns most strongly present in the data (Churchland et al. 2012). PCA has been used to construct a low-dimensional state space for visualizing a dynamic neural trajectory from multiple single-unit activities in the rat medial prefrontal cortex during a working memory task (Zhang et al. 2015). Additionally, feature vectors have been extracted from tactile and proprioceptive afferent activities recorded from the dorsal root ganglion, and the dimensionality of the feature vectors was reduced using PCA (Han et al. 2016, 2017). PCA is a linear feature projection method that projects the coordinates of the original features onto a new small number of coordinates by maximizing the projection variance along the original covariance matrix. PCA can reduce the dimensionality and redundancy of data, but this approach is not always the best way to obtain independent neuronal activities from mixed neural signals. The sciatic nerve innervates the ankle dorsiflexor and plantar flexor muscles and the knee flexor muscles, while the femoral nerve innervates the knee extensor muscles. Various flexor and extensor muscles are activated during ankle and knee movements, and proprioceptors are simultaneously activated in each muscle. The sciatic and femoral nerve neurons of the rabbit are located in the L7 dorsal root ganglia, and afferent signals are transmitted independently through the individual neuronal fascicles (Palumbo et al. 2004; Puigdellívol-Sánchez et al. 1998). When proprioceptive afferent signals are recorded from the L7 dorsal root ganglion of the rabbit using multichannel microelectrodes, each channel of the electrode is contacted by one or more individual neurons of the sciatic or femoral nerves (Han et al. 2017). Consequently, the recorded neural signals can be represented as a linear combination of independent neuronal activities according to the stochastic contact between the channel of the electrode and the neurons of the sciatic or femoral nerves. In these situations, an independent component analysis (ICA) can be useful to separate independent source signals from the recordings of mixed neural signals.

This study presents the real-time decoding of limb state from proprioceptive afferent signals based on a linear feature projection method composed of projection pursuit and negentropy maximization (PP/NEM) for closed-loop control in an FES system. The PP/NEM algorithm is intended for ICA and is suitable for decomposing independent source signals from linearly mixed recordings (Tesfayesus and Durand 2007). In this study, proprioceptive afferent signals were recorded from the L7 dorsal root ganglion using a multichannel microelectrode during passive ankle and knee joint movements, and the dimensionality of the afferent signals was reduced using the PP/NEM method. A time-delayed Kalman filter, optimized with respect to the time delay between the state and observation variables, was then used to estimate the ankle and knee joint movements. The decoding accuracy of the proposed method was compared with that obtained by other dimensionality reduction methods. The experimental results showed that the PP/NEM algorithm achieved a significantly improved decoding accuracy compared with the other dimensionality reduction methods.

2 Methods

2.1 Signal processing procedure

This study attempted to decode ankle and knee joint movements from proprioceptive afferent activities to generate feedback signals for closed-loop control in FES systems. Figure 1 shows a block diagram of the proposed decoding method for the ankle and knee joint angle estimations. Proprioceptive afferent signals were recorded from the L7 dorsal root ganglion using a 16-channel microelectrode, and

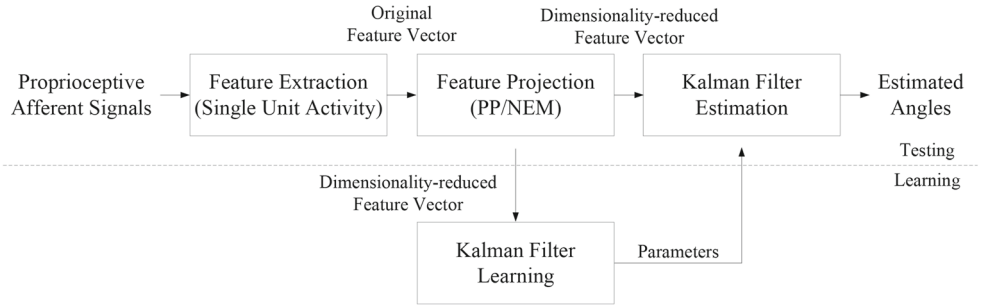

Fig. 1 Block diagram of the proposed decoding method for ankle and knee joint angle estimations from dorsal root ganglion recordings. Single-unit activity was extracted from proprioceptive afferent signals as feature vectors, and the dimensionality of the feature vectors was then reduced using PP/NEM. A time-delayed Kalman filter was constructed using dimensionality-reduced feature vectors in the learning phase, and the ankle and knee joint angles were estimated using the time-delayed Kalman filter in the test phase

ankle and knee joint angles were simultaneously measured as kinematic data. Afferent signals were then segmented considering the interference of stimulus artifacts. A single-unit activity was extracted from each segmented signal as a feature vector, and the dimension of the feature was reduced using the PP/NEM algorithm. All the data were divided into two phases: the learning phase and the test phase. In the learning phase, the time-delayed Kalman filter was constructed to model the relationship between the dimensionality-reduced feature vectors and the kinematic data using a supervised approach and was set to the learning parameter. In the test phase, the ankle and knee joint angles were estimated from the test dataset.

2.2 Data acquisition

All experimental procedures involving animals were approved by the Institutional Animal Care and Use Committee of the Korea Institute of Science and Technology (Certificate number: AP-2013L1001). The experimental protocol was performed in accordance with the recommendations for the care and use of laboratory animals. Neural signals were obtained from five adult male New Zealand white rabbits (weighing 2–2.3 kg). The rabbits were anesthetized via the intramuscular injection of a mixture of ketamine (50 mg/kg) and xylazine (10 mg/kg), and anesthesia was maintained by administering additional doses as needed. The L7 dorsal root ganglion can provide proprioceptive afferent signals from neurons of both the sciatic and femoral nerves during ankle and knee joint movements because the sciatic and femoral nerve neurons are shared in the L7 dorsal root ganglion (Palumbo et al. 2004). Considering the neuroanatomy of the sciatic and femoral nerves in the rabbit, a 16-channel microelectrode (A1x16-5 mm-50-703-CM16, NeuroNexus Technologies, Ann Arbor, MI, USA) was inserted perpendicularly into the right L7 ganglion, where 16 iridium channels, 30 µm in diameter with a 50 µm interchannel distance, were arranged on a 5-mm-long single-shank silicon substrate-based electrode. Reference and ground wires were placed subcutaneously in the back of the rabbit. Neural signals were digitized at 24 kHz and bandpass filtered between 300 and 5000 Hz using a digital data acquisition system (Neuralynx, Tucson, AZ, USA).

Figure 2 shows the experimental setup for obtaining proprioceptive afferent signals and ankle and knee joint angles. A rabbit was positioned on a custom-made stereotaxic frame, and the neutral ankle and knee joint angles were defined as 80 and 130 degrees, respectively, based on the limb's naturally flaccid position. The passive ankle and knee joint movements of the right hind limb in the sagittal plane were generated by servo motors (HS-77BB, Hitec, Korea) and a computer-programmable servo controller. The passive joint motions were adopted from the sit-to-stand maneuver (Mushahwar et al. 2007) and consisted of controlled continuous movement in a sinusoidal pattern at 0.2 Hz. Considering the maximum range of motion of each joint, the ankle and knee joints were passively moved from 50 to 130 degrees and from 80 to 160 degrees, respectively.

Joint angles were measured using wireless inertial measurement unit (IMU) sensors (EBIMU24G, E2BOX, Seoul, Korea). Individual IMU sensors were attached on the right side of the thigh, shank, and foot. The joint angle data were transmitted at a 60-Hz sampling rate from the IMU sensors to a computer. A transistor-transistor logic pulse was used to synchronize the neural signals with the joint angle data at the start and end of the recording sessions. The neural signals and joint angle data were collected from five rabbits during passive ankle and knee joint movements for ten sessions; each session continued for 20 s and consisted of alternating motions of ankle dorsiflexion and plantar flexion and knee flexion and extension. The data acquisition procedures have been described in more detail in a previous study (Han et al. 2017).

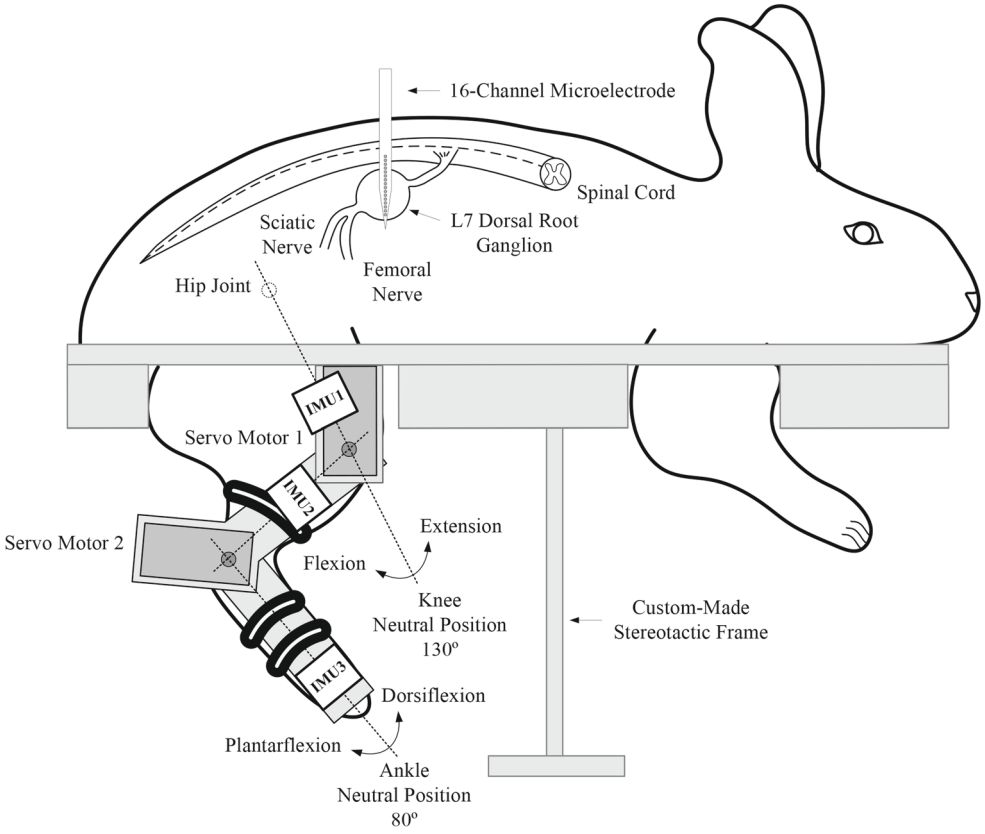

Fig. 2 Experimental setup for dorsal root ganglion recordings during passive ankle and knee joint movements. Proprioceptive afferent signals were recorded using a 16-channel microelectrode, which was inserted perpendicularly into the L7 dorsal root ganglion. Concurrently, ankle and knee joints angles were measured using IMU sensors

2.3 Feature extraction

This study assumed that the ankle and knee joint movements were generated by electrical stimulation at a 60-Hz stimulation repetition frequency with 200-μs charge-balanced biphasic pulses (Han et al. 2017). Electrical stimulation creates stimulus artifacts and contaminates neural signals. To eliminate this interference, a blanking process was applied in synchronization with the stimulation repetition frequency for a duration of 1 ms (Holinski et al. 2013). Thus, interference-free neural signals could be obtained between the applications of two blanking processes. The data window was defined as a period of 15.66 ms corresponding to the time between the blanking processes, and the window increment was set to 16.66 ms based on the stimulation repetition frequency of 60 Hz.

Feature vectors were constructed from single-unit activity, which was defined as the number of spikes from individual neurons during each data window period. Multiple spikes were detected based on threshold crossing events in the data window of each channel, and the threshold was computed as the mean of the baseline noise pulse, which was three times the standard deviation of the mean value for each channel. Each spike consisted of 38 sample points with a spike duration of 1.6 ms, and the refractory period was set to 0.5 ms to prevent double counting of the same spike. Spike sorting was performed based on a PCA and *k*-means clustering to discriminate individual spikes from multiple spikes. A PCA can project the original spike data onto a new small number of coordinates by a linear orthogonal transformation. *k*-means clustering is a commonly used data clustering technique, in which a dataset is partitioned into *k* clusters by minimizing the cost function based on the Euclidean distances between each data point and the cluster centroid. The first three principal components were used as inputs for the *k*-means clustering, and the number of clusters was set to vary from 2 to 4.

The spiking activity of each neuron constructed from spike sorting forms a sequence of discrete events. Additionally, the same neuron may produce quite different spiking activity from trial to trial, even if the experimental conditions are closely reproduced (Cunningham et al. 2009). This variability makes it difficult to estimate the spiking activity accurately. To convert noisy discrete data into denoised continuous time series data, the spiking activity was smoothed using a fourth-order Butterworth low-pass filter with a cut-off frequency at 0.4 Hz.

2.4 Feature projection

Once feature vectors were obtained using the feature extraction method, feature projection was then performed to

reduce the dimensionality of the features. Feature projection produces low-dimensional data from high-dimensional data while retaining the information of interest. Three different linear feature projection methods were investigated to reduce the dimensionality of the feature vectors: PP/NEM, PCA, and factor analysis (FA).

Projection pursuit (PP) linearly transforms the feature vectors to search for the directions of interest in a low-dimensional subspace. PP can be expressed as

$$\mathbf{y} = \mathbf{W}^T\mathbf{x} \tag{1}$$

where $\mathbf{x}$ is the m-dimensional original data, $\mathbf{y}$ is the n-dimensional transformed data, $\mathbf{W}$ is the $m \times n$ matrix. $\mathbf{W}$ is found by minimizing the mutual information between the transformed data. Negentropy was used as an objective function to measure mutual information because entropy is minimized when the mutual information between the transformed data is maximal (Kim and Kim 2003). Consequently, finding an invertible transformation $\mathbf{W}$ that minimizes the mutual information is equivalent to finding directions in which the negentropy is maximized (Hyvarinen 1999). Negentropy, $J(y)$, is defined as

$$J(\mathbf{y}) = H(\mathbf{y}_G) - H(\mathbf{y}) \tag{2}$$

where $H(\mathbf{y})$ is the entropy of a Gaussian random vector $\mathbf{y}$, and $H(\mathbf{y}_G)$ is a Gaussian random vector with the same covariance matrix as $\mathbf{y}$. Minimizing the mutual information of the transformed data $\mathbf{y}$ is the same as finding directions for maximizing negentropy. The value of $\mathbf{W}$ was founded by maximizing $J(\mathbf{y})$, which was implemented using a batch-type learning algorithm based on the PP/NEM method (Hyvarinen 1999; Kim and Kim 2003). With this approach, the original data $\mathbf{x}$ is centered and whitened for computational simplicity, where centering is the subtraction of the average value of $\mathbf{x}$ to generate the zero mean, and whitening is a linear transformation that decorrelates and normalizes $\mathbf{x}$ to set the unit variance. A new vector $\tilde{\mathbf{x}}$ is obtained by using the eigenvalue decomposition of the covariance matrix $E\{\mathbf{x}\mathbf{x}^T\}$=$\mathbf{E}\mathbf{D}\mathbf{E}^T$, where $\mathbf{E}$ is the orthogonal matrix of the eigenvectors of $E\{\mathbf{x}\mathbf{x}^T\}$, and $\mathbf{D}$ is the diagonal matrix of the eigenvalues of $E\{\mathbf{x}\mathbf{x}^T\}$. One PP direction, $\mathrm{y}_i = \mathbf{w}^T\mathbf{x}$, can be obtained by maximizing the function $J_G(\mathbf{w})$ given by

$$J_G(\mathbf{w}) = [E\{G(\mathbf{w}^T\mathbf{x})\} - E\{G(\nu)\}]^2 \tag{3}$$

where G is a non-quadratic function, and ν is a Gaussian variable of zero mean and unit variance. The optimum projection direction can be calculated as

$$\begin{aligned}\mathbf{w}^+ &= E\{\mathbf{x}g(\mathbf{w}^T\mathbf{x})\} - E\{g'(\mathbf{x}^T\mathbf{x})\}\mathbf{x}\\ \mathbf{w}^{\text{new}} &= \mathbf{w}^+/\|\mathbf{w}^+\|\end{aligned} \tag{4}$$

where g is approximated given that $g_1(y) = tanh(a_1 y)$, $g_2(y) = y\exp(-a_2 y^2/2)$, or $g_3(y) = y^3$ are suitable choices for a contrast function, and $1 \leq a_1 \leq 2$, or $a_2 \approx 1$ are constrants. The equation is iterated until the one direction of optimal projection is found. To find more than one direction of projection, a newly found direction of projection is estimated individually based on a Gram-Schmidt orthogonalization, which is performed for every iteration as follows:

$$\begin{aligned}\mathbf{w}_{n+1}^+ &= \mathbf{w}_{n+1} - \sum_{j=1}^{n}(\mathrm{w}_{n+1}^T\mathrm{w}_j)\mathrm{w}_j\\ \mathbf{w}_{n+1}^{\text{new}} &= \mathbf{w}_{n+1}^+/\|\mathbf{w}_{n+1}^+\|.\end{aligned} \tag{5}$$

In this study, $g(y) = y\exp(-a_2 y^2/2)$ was used as a contrast function, and an n-PP direction was extracted as a dimensionality-reduced feature vector. Therefore, the m-dimensional feature vector was projected onto the n-dimensional subspace.

PCA has been widely used in multivariate data analysis for dimensionality reduction and feature extraction, this type of analysis converts a set of correlated observed variables into a new set of uncorrelated variables by a linear orthogonal transformation that maximizes the variance along the axis of principal components. According to the formula $\mathbf{y} = \mathbf{W}^T\mathbf{x}$, the feature vectors correspond to the set of correlated observed variables $\mathbf{x}$, and the dimensionality-reduced feature vectors correspond to the new set of uncorrelated variables $\mathbf{y}$. First, an $m \times n$ covariance matrix was constructed from the feature vectors, and the eigenvalues and eigenvectors were calculated from this covariance matrix. Then, the n eigenvectors corresponding to the n largest eigenvalues were selected to set the rows of the $\mathbf{W}$ matrix. The first n principal components were used to reduce the dimensionality, and thus, the m-dimensional feature vector was projected onto the n-dimensional subspace.

FA is an exploratory data analysis method that represents observed variables as a linear combination of the latent variables plus Gaussian error. FA is defined by Rubin and Thayer (1982) as

$$\mathbf{x} = \mathrm{Z}\Lambda + \varepsilon \tag{6}$$

where $\mathbf{x}$ is the observed variables, Z is the factor matrix, Λ is the factor loading matrix, and ε is the Gaussian noise. The feature vectors correspond to the observed variables $\mathbf{x}$. The factors corresponding to the n largest factor loadings were selected to reduce the dimensionality, and the m-dimensional feature vector was thus projected onto the n-dimensional subspace.

2.5 Neural decoding

The relationship between proprioceptive afferent signals and limb states is a nonlinear dynamic (Prochazka 2015). It is difficult to describe a nonlinear model using a Kalman filter, which is a linear estimator, but the Kalman filter is commonly used as a decoding method because a linear model has the advantages of a low computational cost and suitability for real-time applications. In this study, a time-delayed Kalman filter was used to improve the decoding performance, where a time-delay term was added for the state and observation (Han et al. 2017). Latent state variables were predicted to be a linear dynamic system modeled in the state at a previous time plus Gaussian noise, and the observed variables were assumed to be a linear dynamic system modeled in the state variables plus the Gaussian noise. The state and observation models were defined as

$$\begin{aligned} \mathrm{y}_{t+1} &= \mathbf{A}\mathrm{y}_t + w \\ \mathrm{x}_t &= \mathbf{H}\mathrm{y}_t + v \end{aligned} \tag{7}$$

where $\mathrm{y}_t = (y_t, y_{t-1}, \cdots, y_{t\text{-}p})$ and $\mathrm{x}_t = (x_t, x_{t-1}, \cdots, x_{t\text{-}p})$ are the state and observation variables at time t with a p-order time delay, respectively, and w and v are the process and measurement noises, respectively. $\mathbf{A}$ and $\mathbf{H}$ are the coefficient matrices of the state and observation models, respectively. The w and v values were assumed to be zero mean and normally distributed. $\mathbf{W}$ and $\mathbf{V}$ are the covariance matrices of the process and measurement noises, respectively. The ankle and knee joint angles with a p-order time delay correspond to the state variables, whereas the three-dimensional reduced feature vector with a p-order time delay corresponds to the observed variables. The values of $\mathbf{A}$ and $\mathbf{H}$ were estimated from the learning data using a least-squares estimation (Wu et al. 2004). To estimate the ankle and knee joint angles from this decoding model, the estimate of $\hat{\mathrm{y}}_t$ was obtained using the following equation:

$$\begin{aligned} \hat{\mathrm{y}}_{t,t-1} &= \mathbf{A}\hat{\mathrm{y}}_{t-1} \\ \mathbf{P}_{t,t-1} &= \mathbf{A}\mathbf{P}_{t-1}\mathbf{A}^T + \mathbf{W} \\ \mathbf{K}_t &= \mathbf{P}_{t,t-1}\mathbf{H}^T(\mathbf{H}\mathbf{P}_{t,t-1}\mathbf{H}^T + \mathbf{V})^{-1} \\ \hat{\mathrm{y}}_t &= \hat{\mathrm{y}}_{t,t-1} + \mathbf{K}_t(\mathrm{x}_t - \mathbf{H}\hat{\mathrm{x}}_{t,t-1}) \\ \mathbf{P}_t &= (\mathbf{I} - \mathbf{K}_t\mathbf{H})\mathbf{P}_{t,t-1} \end{aligned} \tag{8}$$

where $\hat{\mathrm{y}}_{t,t-1}$ is the a priori estimate from the previous time, $t-1$, and $\mathbf{P}_{t,t-1}$ is the a priori error covariance matrix. $\hat{\mathrm{y}}$ is the posteriori estimate updated using the $\hat{\mathrm{y}}_{t,t-1}$ and x_t values. $\mathbf{P}_t$ is the posteriori error covariance matrix, and $\mathbf{K}_t$ is the Kalman gain matrix.

2.6 Performance evaluation

The decoding performance of the proposed method was evaluated in estimating ankle and knee joint angles from proprioceptive afferent activities. The proprioceptive afferent signals during passive movements of the ankle and knee joints were recorded from the L7 dorsal root ganglion, and the data window was segmented to 15.66 ms based on the artifact-blanked signals. The single-unit activity was extracted as feature vectors, and the dimensionality of the feature vectors was then reduced to 3 using the PP/NEM method. Dimensionality-reduced feature vectors were then used as inputs for the time-delayed Kalman filter, which was optimized for the time delay of the state and observation variables.

The total dataset was collected during ten sessions for each of five rabbits, and the decoding accuracy was evaluated using a 10-fold cross-validation. Among the ten sessions for each rabbit, one session was randomly selected as the test data, and the remaining nine sessions were used as learning data. The decoding accuracy was calculated based on the test dataset, and this procedure was repeated ten times. The coefficient of determination, R^2, which provides the variation between the measured and estimated values was used to evaluate the decoding accuracy. R^2 is defined as

$$R^2 = 1 - \frac{\sum_{t=1}^{T}(\mathrm{y}_t - \hat{\mathrm{y}}_t)^2}{\sum_{t=1}^{T}(\mathrm{y}_t - \bar{\mathrm{y}})^2} \tag{9}$$

where y_t and $\hat{\mathrm{y}}_t$ are the measured and estimated values at time t, respectively, and $\bar{\mathrm{y}}$ is the mean of y_t in the time interval t=1 to T. T is the number of test datasets. The total decoding accuracy was calculated as the mean of the accuracy among the five rabbits. To remove the effect of differences among the rabbits, a two-way analysis of variance (ANOVA) was used to assess the statistical significance, and Tukey's multiple comparison was used for the post hoc analysis. A confidence level of 95% ($p < 0.05$) was considered to indicate a significant difference. All statistical analyzes were performed using SPSS 15.0 (SPSS Science, Chicago, IL, USA).

2.7 Comparison of different dimensional features

The effect of different dimensional features on the decoding accuracy was investigated. The three-dimensional feature vectors determined by PP/NEM were compared to those of different dimensional feature vectors: the one-, two-, and five-dimensional feature vectors. For the Kalman filter, the four different dimensional reduced feature vectors with a second-order time delay were used as the state variables, and two-dimensional ankle and knee joint angles

with a second-order time delay were used as the observed variables.

2.8 Comparison of different delay orders

The time-delayed Kalman filter includes a time-delay for the state and observed variables. To determine the optimal delay orders, the three-dimensional reduced feature vectors determined by PP/NEM were used as inputs for the Kalman filter, and the decoding accuracy was compared among first-, second- and third-order time delays, where the delay order of the state and the observation were assumed to be equal.

2.9 Comparison of different feature projection methods

To select an optimal feature projection method for estimating the ankle and knee joint angles, the decoding accuracy was compared among the different feature projection methods: PP/NEM, PCA, and FA. For the Kalman filter, three-dimensional reduced feature vectors with a second-order time delay were used as the state variables, and two-dimensional ankle and knee joint angles with a second-order time delay were used as the observed variables.

2.10 Decoding performance of the proposed method

To implement a real-time decoding of ankle and knee joint movements, the processing time should be less than the window increment, which was set to 16.66 ms regarding the maximum processing capability. The processing time of the proposed method was monitored for the feature extraction, feature projection, and neural decoding of the test dataset. The experiment was implemented offline in MATLAB R2015b (MathWorks, Inc., Natick, MA, USA) on an Intel®Core™ i-3 4100M 2.5-GHz PC with 4 GB of RAM running on a Windows 7 64-bit operation system.

3 Results

3.1 Proprioceptive afferent activity during passive ankle and knee joint movements

Muscle spindle afferents in deeply anesthetized animals are rarely fired at substantial rates during passive joint movements because variations in the fusimotor drive and muscle contraction are almost absent in the anesthetized condition. However, afferents in tendons are sensitive to changes in the muscle force by activation of the motor unit. Accordingly, neural signals recorded during passive ankle and knee joint movements in the anesthetized state may be mostly due to the activity of the muscle spindles corresponding to the stretched muscles, and the rate of firing is reduced compared to the unanesthetized state (Prochazka 2015; Prochazka and Ellaway 2012).

Figure 3 shows representative examples of recorded neural signals that were obtained from rabbit A during passive ankle and knee joint movements. The top plot shows the kinematics of the limb movements, while the second plot shows the ankle and knee joint angle data, respectively. The third plot shows the representative five channels of neural signals recorded from the L7 dorsal root ganglion. Different hashes denote different neurons. The bottom plot shows the spike trains of the five channels. The black, red, blue, green, and orange single units are derived from channel 1, channel 2, channel 3, channel 4, and channel 5, respectively. Neural activities changed according to the joint movements. Proprioceptors of the ankle dorsiflexor and plantar flexor muscles are activated during ankle plantarflexion and dorsiflexion, respectively, whereas proprioceptors of the knee flexor and extensor muscles are activated during knee extension and flexion, respectively. Consequently, the single units during ankle dorsiflexion and knee flexion could be proprioceptive afferents from the ankle plantar flexor and knee extensor muscles, such as triceps surae and the quadriceps, whereas the single units during ankle plantar flexion and knee extension are expected to be proprioceptive afferents from the ankle dorsiflexor and knee flexor muscles, such as the tibialis anterior and hamstrings. These patterns of neuronal firing were observed repeatedly according to the movements of the ankle and knee joints and were used to estimate the ankle and knee joint angles.

Table 1 shows the number of individual neurons discriminated from among multiple neurons by spike sorting. For each of the five rabbits, neural signals were simultaneously recorded from 9 to 14 channels of the electrode during the ankle and knee joint movements, and 2 to 4 individual neurons were detected on each channel. Based on the spike sorting, 21 to 37 individual neurons were obtained from each rabbit, and the number of spikes for the individual neuron in each data window was used as a feature vector. Therefore, the dimensionality of the original features m was between 21 and 37.

3.2 Comparison of different dimensional features

Tables 2 and 3 list the decoding accuracies of the different dimensional features used to estimate the ankle and knee joint angles, respectively. For the ankle angle estimations, the three-dimensional feature vectors had a higher decoding accuracy than those of the one- ($p < 0.01$) and two-dimensional feature vectors ($p < 0.01$). For the knee angle estimations, the three-dimensional feature vectors also had

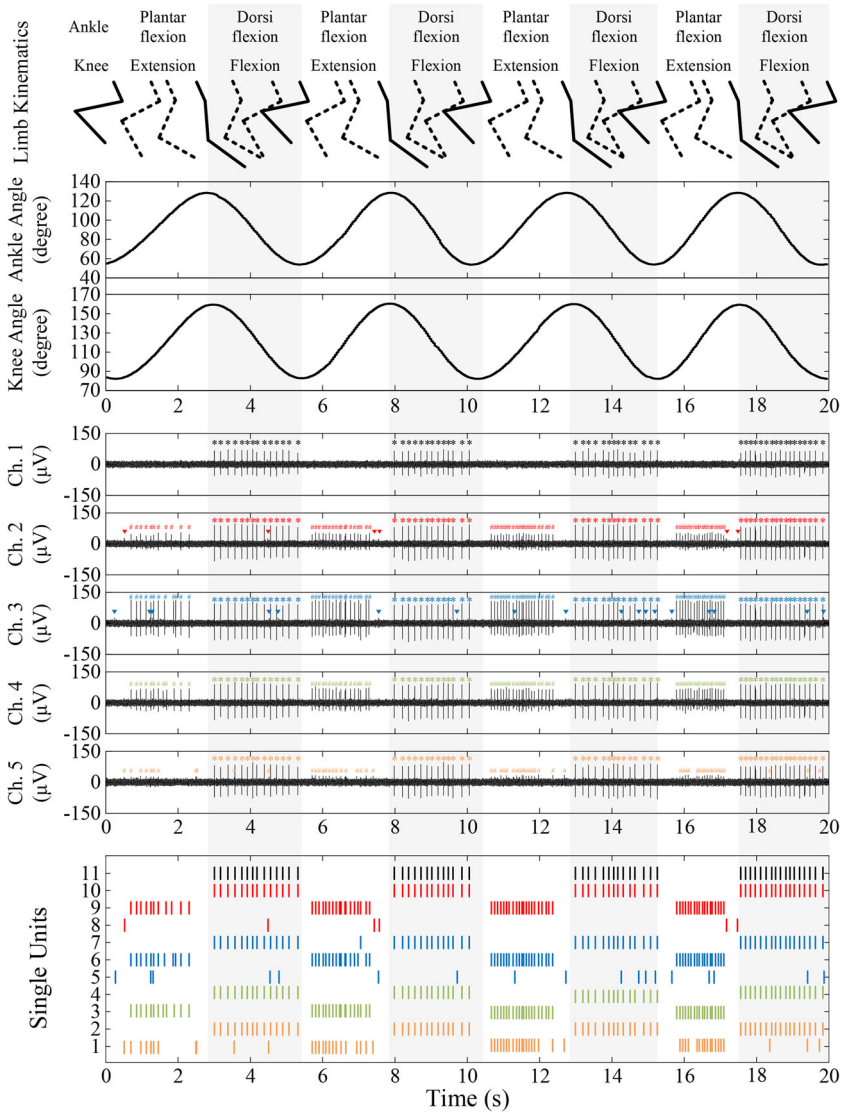

Fig. 3 Typical examples of recorded ankle and knee joint angles and single-unit activity from rabbit A. Ankle and knee joints were moved in a sinusoidal pattern at 0.2 Hz considering the maximum range of motion of each joint. The spike trains were isolated from multiple spikes by spike sorting, where each row represents the activity of an individual neuron in response to the ankle and knee joint movements. The black, red, blue, green, and orange single units are derived from channel 1, channel 2, channel 3, channel 4, and channel 5, respectively

a higher decoding accuracy than those of the one- ($p < 0.01$) and two-dimensional feature vectors ($p < 0.01$). Meanwhile, there were no significant differences in the decoding accuracies between three- and five-dimensional feature vectors for both the ankle and knee joint angle estimations. The decoding accuracy was not improved by the addition of a dimensionality of more than three. This study focused on reducing the dimensionality of the feature vectors while preserving the feature of interest to provide useable information for estimating ankle and knee joint angles. Thus, the three-dimensional reduced feature vectors were used to decode the ankle and knee joint movements.

Table 1 Spike sorting results for each rabbit

Rabbit	A	B	C	D	E
Number of recording channels	14	14	9	9	10
Number of individual neurons	37	32	21	29	21

Table 2 Decoding accuracy with respect to ankle joint movement for different dimensional features

Rabbit	$1-D$	$2-D$	$3-D$	$5-D$
A	0.8186	0.8582	0.8788	0.8699
B	0.7596	0.7980	0.8787	0.8060
C	0.7840	0.8182	0.9497	0.8445
D	0.8568	0.8921	0.9316	0.9270
E	0.8814	0.8952	0.8830	0.9457
Mean	0.8221	0.8524	0.9044	0.8786
±SD	±0.1135	±0.0931	±0.0594	±0.0901

Table 3 Decoding accuracy with respect to knee joint movement for different dimensional features

Rabbit	$1-D$	$2-D$	$3-D$	$5-D$
A	0.8182	0.8578	0.8776	0.8658
B	0.7517	0.7931	0.8736	0.7975
C	0.7899	0.7946	0.9311	0.8365
D	0.8712	0.8744	0.9172	0.9127
E	0.8688	0.8866	0.8754	0.9350
Mean	0.8200	0.8413	0.8950	0.8695
±SD	±0.1196	±0.1056	±0.0656	±0.0988

Table 5 Decoding accuracy with respect to knee joint movement for different delay orders

Rabbit	$1^{st}-order$	$2^{nd}-order$	$3^{rd}-order$
A	0.8940	0.8776	0.8168
B	0.8100	0.8736	0.8029
C	0.9193	0.9311	0.9389
D	0.8797	0.9172	0.8743
E	0.8822	0.8754	0.9258
Mean±SD	0.8770±0.0799	0.8950±0.0656	0.8717±0.1182

3.3 Comparison of different delay orders

Tables 4 and 5 list the decoding accuracies of the different delay orders used to estimate the ankle and knee joint angles, respectively. For the ankle angle estimations, the second-order time delay was significantly higher for decoding accuracy than the first- ($p < 0.05$) and third-order time delays ($p < 0.05$). For the knee angle estimations, the decoding accuracy of the second-order time delay was approximately 1.80% and 2.33% ($p < 0.05$) higher than that of the first- and third-order time delays, respectively, but the difference between the first- and second-order time delays was not significant ($p > 0.05$). This result indicates that a second-order time delay provides a significantly better decoding performance than those obtained using the other time delay orders in the ankle angle estimations but a significantly better or similar decoding performance in the knee angle estimations. Thus, the second-order time delay was selected as an optimal delay order in our decoding application.

3.4 Comparison of different feature projection methods

Tables 6 and 7 show the decoding accuracies of the different feature projection methods for the ankle and knee joint angle estimations, respectively. The PP/NEM method obtained a decoding accuracy of 0.9044 ± 0.0594 and 0.8950 ± 0.0656 for the ankle and knee angle estimations, respectively, which was significantly better than the PCA and FA results. The decoding accuracy of the PP/NEM method was approximately 6.29% ($p < 0.01$) and 4.29% ($p < 0.05$) higher than those of the PCA and FA methods for the ankle angle estimation, respectively, and approximately 7.51% ($p < 0.01$) and 8.53% ($p < 0.01$) higher than those of the PCA and FA methods for the knee angle estimation, respectively. This result suggests that the PP/NEM approach has better decoding performance than the PCA and FA methods.

3.5 Decoding performance of the proposed method

Figure 4 shows an example of the decoding results of rabbit D obtained using the proposed method. The top plot shows the spike trains of neuronal activity during the limb movements, and the second plot shows the dimensionality-reduced feature vectors corresponding to the three independent components. The bottom plot shows the estimation results of the ankle and knee joint angles obtained using the Kalman filter integrated with a second-order time delay for the state and observed variables. The black solid line denotes the ankle and knee joint angles measured by IMU sensors, and the blue solid line denotes the estimated angles using the proposed method. The means and standard deviation of the R^2 values between the measured and estimated angles in the five rabbits were

Table 4 Decoding accuracy with respect to ankle joint movement for different delay orders

Rabbit	$1^{st}-order$	$2^{nd}-order$	$3^{rd}-order$
A	0.8725	0.8788	0.8285
B	0.8106	0.8787	0.7954
C	0.9147	0.9497	0.9253
D	0.8639	0.9316	0.8914
E	0.8732	0.8830	0.9319
Mean±SD	0.8670±0.0777	0.9044±0.0594	0.8745±0.1041

Table 6 Decoding accuracy with respect to ankle joint movement for the different feature projection methods

Rabbit	PP/NEM	PCA	FA
A	0.8788	0.7990	0.8373
B	0.8787	0.8223	0.8579
C	0.9497	0.8604	0.8124
D	0.9316	0.8864	0.8992
E	0.8830	0.8392	0.9004
Mean±SD	0.9044±0.0594	0.8415±0.1082	0.8615±0.1112

Table 7 Decoding accuracy with respect to knee joint movement for the different feature projection methods

Rabbit	PP/NEM	PCA	FA
A	0.8776	0.7615	0.7425
B	0.8736	0.8451	0.8045
C	0.9311	0.7469	0.7458
D	0.9172	0.9159	0.8642
E	0.8754	0.8303	0.8016
Mean±SD	0.8950±0.0656	0.8199±0.1387	0.8097±0.1318

0.9044 ± 0.0594 and 0.8950 ± 0.0656 for the ankle and knee joint movements, respectively.

The processing time of the proposed method for estimating ankle and knee joint angles is shown in Table 8. Each decoding result was generated within 10.969 ms, which is less than the window increment of 16.66 ms, and therefore, the proposed method can be applied to the real-time decoding of limb state to provide sensory feedback in a closed-loop FES system.

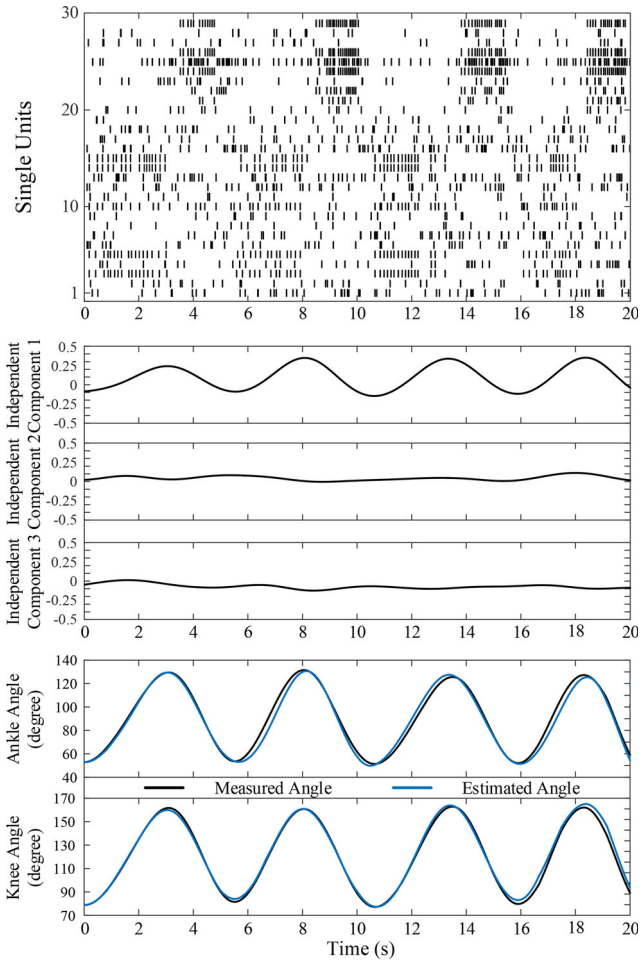

Fig. 4 A typical example of a decoding result from rabbit D using the proposed method. The top plot shows the spike trains during ankle and knee joint movements, and the second plot shows the three independent components obtained from smoothed single-unit activity using PP/NEM. The bottom plot is the decoding result of the ankle and knee joint angle estimates. The black and blue solid lines denote the measured and estimated angles, respectively

Table 8 Processing time for the proposed method

Processes	Processing time (ms)
Feature extraction	4.4085
PP/NEM	1.351×10^{-2}
Kalman filter	6.548
Total	10.969

4 Discussion

Sensory feedback-based closed-loop control of FES systems can be useful for restoring lost motor function in paralyzed patients, and neural activities such as cutaneous and proprioceptive afferents have been investigated as a natural source of sensory feedback for FES systems. Many studies have been conducted to extract sensory information from peripheral nervous systems (Chu et al. 2013; Raspopovic et al. 2010; Tesfayesus and Durand 2007; Yoo and Durand 2005). For example, a single-channel cuff electrode was used to identify different types of afferent stimuli from sciatic nerve recordings of anesthetized rats (Raspopovic et al. 2010). This was based on the fact that different types of afferents are propagated along different types of nerve fibers with different conduction velocities. The cuff electrode can detect mixed neural activity from the nearest nerve fibers, which are primarily in contact with the electrode channel. Thus, the activity of single axons is difficult to extract from recorded signals using a cuff electrode. These limitations can be partly overcome using multichannel cuff electrodes, which were developed to improve selectivity and distinguish between different active fibers (Yoo and Durand 2005), but multichannel cuff electrodes also cannot make contact with a targeted axon within a nerve bundle, thereby providing the aggregate neural activities of multiple fascicles and reducing selectivity compared to other intrafascicular multichannel electrodes.

In other studies, the sensory information of limb movement was extracted from dorsal root ganglion recordings. Sensory neurons are gathered in the dorsal root ganglion, making it an attractive location to extract sensory information. For example, sensory information was extracted from recorded afferent signals using a microelectrode array implanted in the L7 dorsal root ganglion of a walking cat, and limb kinematics were decoded using a multivariate linear regression model (Weber et al. 2007). Another study used a neuro-fuzzy

algorithm to estimate limb kinematics from the recordings of up to 100 electrodes in the L6 and L7 dorsal root ganglion to improve decoding performance (Rigosa et al. 2011). Limb position was estimated using neural signals obtained with penetrating microelectrode arrays in the dorsal root ganglia and multi-state walking patterns were generated by a closed-loop FES control system based on limb position feedback (Bruns et al. 2013). Neural interface technology is being developed to record hundreds of discriminable neurons simultaneously, which can lead to improvement in the quality of information extracted from neural signals. However, increasing the available information requires more computational effort proportionally. In addition, neural interface systems ultimately need to be implanted in the body. The wireless transmission of data is limited under the strict power limits of implantable wireless systems, and therefore, data reduction is important for implantable neural systems (Gibson et al. 2012). Dimensionality reduction methods can be commonly applied to population neural activity and offer practical advice about interpreting their outputs (Cunningham and Byron 2014). Therefore, we believe that dimensionality reduction is important to reduce the amount of data and the processing time for real-time implementation of neural interface systems.

The goal of this study was to propose a real-time decoding method for proprioceptive afferent signals using linear feature projection to allow closed-loop control in an FES system. The proposed decoding method was composed of the PP/NEM approach and a time-delayed Kalman filter. PP/NEM is a linear feature projection method that can extract features and reduce the dimensionality of large-scale data to a low amount of data without losing useful information. PP/NEM has also been widely used for blind source separation; linearly mixed independent source signals can be recovered from their multiple-channel recordings using ICA. The feasibility of ICA based on PP/NEM has been investigated to extract fascicular source signals from peripheral afferent recordings for closed-loop control in FES (Tesfayesus and Durand 2007). The L7 dorsal root ganglion of the rabbit contains neurons of both the sciatic and femoral nerves, and the distributions of their neurons are topographically different (Palumbo et al. 2004; Puigdellívol-Sánchez et al. 1998). The sciatic and femoral nerves include afferent fibers arising from different muscles corresponding to the ankle and knee joint movements, and these afferent fibers are organized into individual fascicles that carry *kinesthesia* information. When a microelectrode was inserted into the L7 dorsal root ganglion, each channel of the electrode was directly placed around the different neurons, achieving selectivity of both the sciatic and femoral nerve neurons. Therefore, the neural signals from the L7 dorsal root ganglion recorded using a multichannel microelectrode could be regarded as a linear mixture of independent neuronal signals, and the statistical properties of the recorded neural signals from the dorsal root ganglion could meet the PP/NEM application requirements for dimensionality reduction.

The PP/NEM method exhibited a significantly better decoding performance than that of the PCA and FA methods. A PCA determines a set of new uncorrelated latent variables from observed variables by maximizing the projection variance using the eigenvalue of the covariance matrix. An FA describes the observed variables as a mixed model of factors and factor loadings. Both PCA and FA can generate low-dimensional uncorrelated variables from high-dimensional data, but uncorrelated variables do not always indicate independent variables. PP/NEM estimates independent source signals by measuring the negentropy of estimated signals, which is equivalent to the degree of mutual independence. Mutual independence can be achieved by maximizing the negentropy of the estimated source signals. Consequently, the PP/NEM method can separate independent source signals from the recorded neural signals and reduce the dimensionality, including most informative features, thereby achieving higher decoding accuracy than PCA and FA.

A Kalman filter provides a recursive estimate of state variables from observed variables, which assumes that the state is linearly related to the observation. As a linear decoding algorithm, a Kalman filter has the advantage of being fast and stable in decoding behavioral trajectories from neural activity and has been successfully used as a neural decoding method (Wu et al. 2004). The time-delayed Kalman filter, which was constructed with a time delay for the state and observed variables, was used to estimate ankle and knee joint angles. The time delay can enhance the learning capability of temporal and spatial patterns and, thereby, play a key role in improving dynamic decoding performance. Generally, a higher delay order of state and observation can represent more temporal information. However, as the delay order increases, the input dimensionality increases and more computational effort is required. Consequently, an appropriate delay order should be selected to reduce the processing time and improve decoding performance. Among the delay orders, a second-order time delay achieved a higher performance than the other delay orders in our experiments.

The proposed method consisted of PP/NEM and a Kalman filter, where PP/NEM and the Kalman filter are the linear feature projection and linear decoding methods, respectively. These linear methods are fast and simple to use and adequate for real-time processing. In closed-loop FES systems, the sensory feedback signals are determined continuously without a delay time, and stimulation pulses are generated based on the feedback signals for controlling limb movements. The processing time of the proposed

method satisfied these real-time constraints. This result suggests that the proposed method can accurately estimate the ankle and knee joint angles in real time and is suitable for closed-loop FES systems.

Accurate estimates of the firing rates of individual neurons are complicated because neuronal activity is highly variable. Thus, many studies have decoded limb movements from the smooth estimates of the firing rate (Cunningham et al. 2009). In this study, the feature vector was constructed from the smoothed firing rates using a fourth-order Butterworth low-pass filter with a cut-off frequency of 0.4 Hz, considering limb movement generated by the sinusoidal pattern of 0.2 Hz. Limb movement of 0.2 Hz is very slow compared to normal movements. Choosing a different cut-off frequency might produce a significantly different decoding accuracy. Therefore, in the case of realistic joint angle variations of normal movement, a greater information bandwidth than we used will be required to achieve high decoding performance and appropriate cut-off frequency of the low-pass filter should be selected according to the speed of movement.

In FES systems, electrical stimulation can produce two types of stimulus artifacts and contaminate neural signal recordings. A first artifact is concurrently appeared in the recording channels due to electrical stimulation, and a second artifact is induced directly by afferent fibers activation and appeared in the dorsal root ganglion after a short latency (∼2-5 ms) corresponding to the nerve conduction delay from stimulation site to the dorsal root ganglion (Bruns et al. 2013). When applying blanking to eliminate stimulus artifacts, an appropriate blanking period should be chosen because a short blanking duration cannot avoid artifacts, whereas a long blanking duration increases the loss of information and decreases the available signal length. In this study, we applied a 1 ms blanking period synchronized with the stimulation repetition frequency in the recordings to avoid the stimulus artifacts referred from the previous study of actual intraspinal microstimulation (ISMS) (Holinski et al. 2013). ISMS required smaller current amplitude levels than other intramuscular stimulations to induce limb movement, and almost all stimulus artifacts were successfully removed using a 1 ms blanking period (Holinski et al. 2013). Another study achieved closed-loop FES control of hind limb based on the limb position feedback from dorsal root ganglion recordings with a 2 ms blanking period (Bruns et al. 2013). Electrical artifact evoked by stimulation can be effectively removed by a simple artifact rejection method with relatively short blanking period. However, these blanking periods are generally inappropriate to eliminate the stimulus artifact of neuronal activity that is induced by afferent fibers activation in typical intramuscular or neuromuscular approaches for FES control. Stimulation-induced neuronal activity would likely affect decoding accuracy, and therefore many studies have used a longer blanking period that can include this artifact (Chu et al. 2013; Song et al. 2017). For example, ankle movement was induced by neuromuscular stimulation, and then ankle angle was predicted using sciatic nerve recordings with a 6 ms blanking period (Song et al. 2017). This 6 ms blanking period is presumably long enough to eliminate the interference noise both electrical artifact and stimulation-induced neuronal activity. Further study is necessary to investigate the optimal blanking period for obtaining interference-free neural signals during actual electrical stimulation and the effect of additional neuronal activity induced by electrical stimulation on the decoding accuracy.

In our experiment, the decoding performance of the proposed method was evaluated during passive limb movements in anesthetized rabbits. The afferent signals induced by passive movements may be mostly due to the activity of the muscle spindle, while variations in the fusimotor drive and the mechanical effects of muscle contraction, pennation angle changes, and tendon compliance may be absent (Prochazka 2015). The limb movement was a simple up-down cycling, similar to the sit-to-stand maneuver where the ankle and knee joint move in synchrony. These limb movements differ greatly from a full limb step cycle. In volitional movements of the unanesthetized condition, muscle spindle firing can be strongly influenced by variations in fusimotor drive and muscle contraction. Recorded afferent signals may include not only proprioceptive afferents but also cutaneous afferents responding to contact, skin stretch, and hair movement. These influences change the signal patterns of the afferents signals recorded from the unanesthetized condition and act as noise in the decoding of limb movements. The proposed method could be invalid in a case where the recorded afferent signals are generated from different sensory modalities. To resolve this problem, an additional identification procedure is necessary to discriminate a proprioceptive afferent activity from the recorded afferent signals according to different sensory modalities. In future studies, the proposed decoding method will be directly implemented for real-time decoding of active multi-directional limb movements using dorsal root ganglion recordings to provide sensory feedback signals in closed-loop FES systems.

5 Conclusion

This paper proposed a real-time decoding method for estimating ankle and knee joint angles from proprioceptive afferent signals using a linear feature projection for closed-loop control in FES systems. The proprioceptive afferent signals were recorded from the L7 dorsal root ganglion using a multichannel microelectrode during passive ankle

and knee joint movements, and feature vectors were extracted from the single-unit activities. The dimension of the features was then reduced using the PP/NEM method, which maximizes the negentropy as a measure of statistical independence between signals. A time-delayed Kalman filter was used to estimate the ankle and knee joint angles and showed a high decoding accuracy for both the ankle and knee joint angle estimates. All decoding processes were completed within the real-time constraints. The proposed method might be applicable to providing real-time limb-state feedback in closed-loop FES systems.

Acknowledgements This work was supported in part by a grant of the Next-generation Medical Device Development Program for Newly-Created Market of the National Research Foundation (NRF) funded by the Korean Government, MSIP (No. 2015M3D5A1066100), the convergence technology development program for bionic arm through the NRF funded by the Ministry of Science, ICT & Future Planning (2017M3C1B2085311), the Korea Institute of Science and Technology Institutional Program (2E27980), and the Korea University Grant.

Compliance with Ethical Standards

Conflict of interests The authors declare that they have no conflict of interest.

References

Bruns, T.M., Wagenaar, J.B., Bauman, M.J., Gaunt, R.A., Weber, D.J. (2013). Real-time control of hind limb functional electrical stimulation using feedback from dorsal root ganglia recordings. *Journal of Neural Engineering*, *10*(2), 026,020.

Chu, J.U., Song, K.I., Han, S., Lee, S.H., Kang, J.Y., Hwang, D., Suh, J.K.F., Choi, K., Youn, I. (2013). Gait phase detection from sciatic nerve recordings in functional electrical stimulation systems for foot drop correction. *Physiological measurement*, *34*(5), 541.

Churchland, M.M., Cunningham, J.P., Kaufman, M.T., Foster, J.D., Nuyujukian, P., Ryu, S.I., Shenoy, K.V. (2012). Neural population dynamics during reaching. *Nature*, *487*(7405), 51.

Cunningham, J.P., & Byron, M.Y. (2014). Dimensionality reduction for large-scale neural recordings. *Nature neuroscience*, *17*(11), 1500–1509.

Cunningham, J.P., Gilja, V., Ryu, S.I., Shenoy, K.V. (2009). Methods for estimating neural firing rates, and their application to brain–machine interfaces. *Neural Networks*, *22*(9), 1235–1246.

Gibson, S., Judy, J.W., Marković, D. (2012). Spike sorting: The first step in decoding the brain: The first step in decoding the brain. *IEEE Signal processing magazine*, *29*(1), 124–143.

Han, S., Chu, J.U., Kim, H., Choi, K., Park, J.W., Youn, I. (2016). An unsorted spike-based pattern recognition method for real-time continuous sensory event detection from dorsal root ganglion recording. *IEEE Transactions on Biomedical Engineering*, *63*(6), 1310–1320.

Han, S., Chu, J.U., Kim, H., Park, J.W., Youn, I. (2017). Multiunit activity-based real-time limb-state estimation from dorsal root ganglion recordings. *Scientific Reports*, *7*, 44,197.

Holinski, B., Everaert, D., Mushahwar, V., Stein, R. (2013). Real-time control of walking using recordings from dorsal root ganglia. *Journal of Neural Engineering*, *10*(5), 056,008.

Hyvarinen, A. (1999). Fast and robust fixed-point algorithms for independent component analysis. *IEEE transactions on Neural Networks*, *10*(3), 626–634.

Kim, K.H., & Kim, S.J. (2003). Method for unsupervised classification of multiunit neural signal recording under low signal-to-noise ratio. *IEEE Transactions on Biomedical Engineering*, *50*(4), 421–431.

Mushahwar, V.K., Jacobs, P.L., Normann, R.A., Triolo, R.J., Kleitman, N. (2007). New functional electrical stimulation approaches to standing and walking. *Journal of Neural Engineering*, *4*(3), S181.

Palumbo, M., Valdes, M., Robertson, A., Sheikh, S., Lucas, P. (2004). Posterolateral intertransverse lumbar arthrodesis in the new zealand white rabbit model:: I. surgical anatomy. *The Spine Journal*, *4*(3), 287–292.

Pregowska, A., Szczepanski, J., Wajnryb, E. (2016). Temporal code versus rate code for binary information sources. *Neurocomputing*, *216*, 756–762.

Prochazka, A. (2015). Proprioceptor models. Encyclopedia of computational neuroscience, pp. 2501–2518.

Prochazka, A., & Ellaway, P. (2012). Sensory systems in the control of movement. *Comprehensive Physiology*, *2*, 2615–2628.

Puigdellivól-Sánchez, A., Prats-Galino, A., Ruano-Gil, D., Molander, C. (1998). Sciatic and femoral nerve sensory neurones occupy different regions of the l4 dorsal root ganglion in the adult rat. *Neuroscience letters*, *251*(3), 169–172.

Raspopovic, S., Carpaneto, J., Udina, E., Navarro, X., Micera, S. (2010). On the identification of sensory information from mixed nerves by using single-channel cuff electrodes. *Journal of neuroengineering and rehabilitation*, *7*(1), 17.

Rigosa, J., Weber, D., Prochazka, A., Stein, R., Micera, S. (2011). Neuro-fuzzy decoding of sensory information from ensembles of simultaneously recorded dorsal root ganglion neurons for functional electrical stimulation applications. *Journal of Neural Engineering*, *8*(4), 046,019.

Rubin, D.B., & Thayer, D.T. (1982). Em algorithms for ml factor analysis. *Psychometrika*, *47*(1), 69–76.

Song, K.I., Chu, J.U., Park, S.E., Hwang, D., Youn, I. (2017). Ankle-angle estimation from blind source separated afferent activity in the sciatic nerve for closed-loop functional neuromuscular stimulation system. *IEEE Transactions on Biomedical Engineering*, *64*(4), 834–843.

Stein, R., Aoyagi, Y., Weber, D., Shoham, S., Normann, R. (2004). Encoding mechanisms for sensory neurons studied with a multielectrode array in the cat dorsal root ganglion. *Canadian journal of physiology and pharmacology*, *82*(8-9), 757–768.

Tesfayesus, W., & Durand, D. (2007). Blind source separation of peripheral nerve recordings. *Journal of neural engineering*, *4*(3), S157.

Wagenaar, J., Ventura, V., Weber, D. (2011). State-space decoding of primary afferent neuron firing rates. *Journal of neural engineering*, *8*(1), 016,002.

Weber, D., Stein, R., Everaert, D., Prochazka, A. (2007). Limb-state feedback from ensembles of simultaneously recorded dorsal root ganglion neurons. *Journal of Neural Engineering*, *4*(3), S168.

Weber, D.J., Stein, R.B., Everaert, D.G., Prochazka, A. (2006). Decoding sensory feedback from firing rates of afferent ensembles recorded in cat dorsal root ganglia in normal locomotion. *IEEE Transactions on Neural Systems and Rehabilitation Engineering*, *14*(2), 240–243.

Wolpert, D.M., & Ghahramani, Z. (2000). Computational principles of movement neuroscience. *Nature neuroscience*, *3*(11s), 1212.

Wu, W., Shaikhouni, A., Donoghue, J., Black, M. (2004). Closed-loop neural control of cursor motion using a kalman filter. In: Engineering in Medicine and Biology Society, 2004. IEMBS'04. 26th Annual International Conference of the IEEE, IEEE, vol. 2, pp. 4126–4129.

Yoo, P.B., & Durand, D.M. (2005). Selective recording of the canine hypoglossal nerve using a multicontact flat interface nerve electrode. *IEEE Transactions on Biomedical Engineering*, *52*(8), 1461–1469.

Zhang, X., Yi, H., Bai, W., Tian, X. (2015). Dynamic trajectory of multiple single-unit activity during working memory task in rats. *Frontiers in computational neuroscience*, *9*, 117.